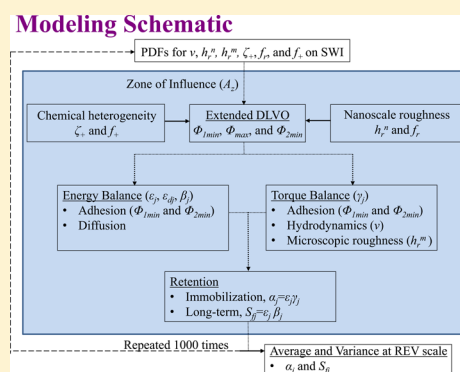


Determining Parameters and Mechanisms of Colloid Retention and Release in Porous Media

Scott A. Bradford^{*,†} and Saeed Torkezaban[‡][†]US Salinity Laboratory, USDA, ARS, Riverside, California 92507, United States[‡]CSIRO Land and Water, Glen Osmond, SA 5064, Australia

Supporting Information

ABSTRACT: A modeling framework is presented to determine fundamental parameters and controlling mechanisms of colloid (microbes, clays, and nanoparticles) retention and release on surfaces of porous media that exhibit wide distributions of nanoscale chemical heterogeneity, nano- to microscale roughness, and pore water velocity. Primary and/or secondary minimum interactions in the zone of electrostatic influence were determined over the heterogeneous solid surface. The Maxwellian kinetic energy model was subsequently employed to determine the probability of immobilization and diffusive release of colloids from each of these minima. In addition, a balance of applied hydrodynamic and resisting adhesive torques was conducted to determine locations of immobilization and hydrodynamic release in the presence of spatially variable water flow and microscopic roughness. Locations for retention had to satisfy both energy and torque balance conditions for immobilization, whereas release could occur either due to diffusion or hydrodynamics. Summation of energy and torque balance results over the elementary surface area of the porous medium provided estimates for colloid retention and release parameters that are critical to predicting environmental fate, including the sticking and release efficiencies and the maximum concentration of retained colloids on the solid phase. Nanoscale roughness and chemical heterogeneity produced localized primary minimum interactions that controlled long-term retention, even when mean chemical conditions were unfavorable. Microscopic roughness played a dominant role in colloid retention under low ionic strength and high hydrodynamic conditions, especially for larger colloids.



INTRODUCTION

An understanding of and ability to predict colloid (microbes, clays, and engineered nanoparticles) retention and release in natural porous media are needed for many industry and environmental applications. Numerous studies from a diversity of disciplines have been conducted on this topic.^{1–6} It is now well-understood that colloid retention and release are dependent on a myriad of incompletely characterized interactions with diverse solid surfaces that are coupled with a multitude of physical, chemical, and microbiological factors.^{7–10} This complexity has led to many conflicting opinions on mechanisms and factors controlling colloid retention and release under unfavorable conditions. As a result, there is still no consensus in the literature on the proper conceptual and/or mathematical framework to describe colloid transport in porous media.^{7–10} In this work, we present an approach to determine fundamental parameters and mechanisms required to describe colloid retention and release processes at the representative elementary volume (REV) scale.

Heterogeneous flow and transport properties that occur at the pore-scale are averaged over a REV to obtain effective lumped parameters for continuum scale models. Colloid transport in porous media has commonly been described at the REV scale using the advective-dispersion equation (ADE)

with a first-order kinetic retention term.^{1,11,12} Colloid filtration theory (CFT) considers the retention rate coefficient to be the product of the colloid mass transfer rate from the bulk aqueous phase to the solid–water interface (SWI) and the colloid sticking efficiency (α).^{13,14} This theory assumes a constant rate of retention over time, implying an infinite retention capacity.¹⁵ However, numerous studies have shown that natural porous media always have a finite retention capacity that depends on the physicochemical conditions.^{16–18} The maximum solid phase colloid concentration (S_{\max}) can be calculated, either experimentally or theoretically, to determine the fraction of the SWI that contributes to colloid retention (S_f).¹⁹ The value of S_f has been found to be small, even under chemical conditions that are predicted to be favorable for retention. Therefore, the retention rate coefficient is expected to decrease with time as available retention sites are filled.^{18–20}

CFT also assumes irreversible colloid retention and negligible colloid release.¹ However, persistent low levels of colloid release are commonly observed under steady-state physicochemical conditions.¹ These observations imply that the

Received: August 17, 2015

Revised: October 19, 2015

Published: October 20, 2015

CFT assumption of irreversible colloid retention may be violated, and the strict interpretation of α as an irreversible sticking efficiency may be flawed. Indeed, the conceptual model of colloid transport, retention, and release can have a strong influence on the physical interpretation of α . For example, if the ADE includes first-order retention and release terms, then the value of α reflects the probability of reversible and irreversible colloid immobilization. This interpretation of α is employed in this work. However, it should be mentioned that the value of α may take on other meanings when considering two-site and two-region models for colloid retention and release.¹⁰

Values of α and S_f are mainly determined in column-scale studies by inverse optimization to experimental breakthrough curves and/or retention profiles.¹⁰ However, these parameters are known to be extremely sensitive to site-specific physicochemical and flow conditions.^{16–18,20} Consequently, predicting colloid retention and release parameters in natural porous media remains a critical challenge. Only a few approaches have been developed to estimate α , and little research attention has been given to the determination of S_f . Several researchers have developed empirical correlations between experimental values of α and physicochemical conditions.^{21–25} Others have attempted to theoretically estimate values of α , and in some cases S_f , by considering fundamental forces and/or torques that act on colloids.^{26–30} However, these correlations and theoretical predictions have not considered the full range of conditions that influence colloid retention and release by neglecting one or more of the following critical factors: nanoscale chemical heterogeneity,^{31,32} nanoscale roughness,^{33–36} microscopic roughness and/or grain–grain contacts,^{27,37} spatial variability in water velocity due to pore space geometry and grain size distribution,³⁸ finite primary and secondary minimum interactions,^{39,40} and/or the ability of colloids to diffuse into or out of minima in the interaction energy profile.^{41,42} Consequently, the above models have had only limited success, and they do not allow for systematic investigation of the full range of retention and release mechanisms.

The objective of this research is to provide a modeling framework to predict values of α and S_f in a porous medium for various physicochemical conditions. The combined effects of nanoscale roughness and chemical heterogeneity, microscopic roughness, solution ionic strength (IS), pore water velocity, and colloid radius on colloid retention and release were subsequently investigated. Results provide valuable insight on controlling mechanisms for retention and release.

■ COLLOID RETENTION AND RELEASE IN THE ZONE OF INFLUENCE

We assume that the colloid of interest has a given size and charge, is spherical in shape, neutrally buoyant, and physically and chemically homogeneous. Furthermore, we assume that the colloid is suspended in a monovalent electrolyte solution with a given IS. In contrast to the colloid, we assume that the surface of the porous medium exhibits wide distributions of nanoscale roughness and chemical heterogeneity as well as microscopic roughness. Hence, conditions for colloid retention and release vary spatially over the SWI. The electrostatic zone of influence (A_z , L^2 where L denotes units of length) refers to the projected area of the colloid on the SWI that effectively contributes to the colloid–SWI interaction energy. Note that A_z is proportional to the colloid radius and the Debye length.⁴³ Below, we discuss the determination of the interaction energy, the energy balance, the torque balance, and values of α and S_f for each individual A_z on the SWI. In

the next section, we discuss the determination of upscale values of α and S_f over the heterogeneous surface of the porous medium.

Interaction Energies. Colloids in an electrolyte solution experience attractive or repulsive interactions energies as they approach the SWI. Theory developed by Derjaguin–Landau–Verwey–Overbeek (DLVO) considers this energy to arise from the superposition of electrostatic and van der Waals interactions.^{44,45} Other non-DLVO interactions may occur due to Born repulsion, hydration and hydrophobic forces, and steric interactions.^{46,47} Nanoscale physical and/or chemical heterogeneity can also have a pronounced influence on colloid interaction energies.^{31–36}

Each A_z on the SWI was assumed to contain a nanoscale roughness fraction (f_r) with a height equal to h_r^n and a positive zeta potential fraction (f_+) that is equal to ζ_+ . The complementary fractions ($1 - f_r$) and $(1 - f_+)$ correspond to a smooth surface and a negative zeta potential ζ_- , respectively. Mean values of the dimensionless interaction energy (Φ) within A_z were subsequently quantified using a linear combination of interaction energies associated with the nanoscale roughness and chemical heterogeneity fractions as³⁵

$$\Phi(h) = (1 - f_r)\Phi_s(h + h_r^n) + f_r\Phi_s(h) \quad (1)$$

where h [L] is the separation distance from the center of A_z at a height h_r^n to the leading face of the colloid center. The dimensionless interaction energy associated with a smooth, nanoscale chemically heterogeneous surface (Φ_s) is given as³⁵

$$\Phi_s(h) = (1 - f_+)\Phi_-(h) + f_+\Phi_+(h) \quad (2)$$

Values of ζ_- and ζ_+ were used to determine the corresponding dimensionless interaction energies for negative (Φ_-) and positive (Φ_+) fractions, respectively. Equations 1 and 2 assume that nanoscale roughness and chemical heterogeneity, respectively, occur directly below the colloid within A_z . All of the above interaction energies considered electrostatics,⁴⁸ retarded London–van der Waals attraction,⁴⁹ and Born repulsion⁵⁰ and assumed a sphere–plate geometry. Equations for these interactions are given in the Supporting Information, Section S1. Figure S1 provides a schematic illustrating the influence of nanoscale roughness and chemical heterogeneity on interaction energies within A_z .

The secondary minimum (Φ_{2min}), the energy barrier (Φ_{max}), and the primary minimum (Φ_{1min}) were subsequently determined for each A_z under a given chemical condition using Boolean logic statements in conjunction with minimum and/or maximum functions over specified intervals in h . As expected, a wide range of interactions is possible for colloids interacting with a heterogeneous surface depending on the nanoscale heterogeneity type, size, and amount.^{26,35,39} Note that the depth of the primary minima is finite when Born repulsion and nanoscale roughness are considered in these calculations.^{39,40} Consequently, five distinct classes of interaction energy profiles were identified that encompass all possible values of Φ_{1min} and Φ_{max} . Figure S2 present examples of interaction energy profiles that are representative of these five classes. The classes ranged from favorable to unfavorable for interaction in a primary minimum and were determined based on values of Φ_{1min} and Φ_{max} . In particular, class 1 has values of $\Phi_{1min} < 0$ and $\Phi_{max} = \text{NA}$; class 2 has values of $\Phi_{1min} < 0$ and $\Phi_{max} < 0$; class 3 has values of $\Phi_{1min} < 0$ and $\Phi_{max} > 0$; class 4 has values of $\Phi_{1min} > 0$ and $\Phi_{max} > 0$; and class 5 has values of $\Phi_{1min} = \text{NA}$ and $\Phi_{max} > 0$. Here, NA denotes not applicable.

Energy Balance. In the absence of water flow, the retention (i.e., immobilization or attachment) and release (i.e., detachment) of colloids interacting with the SWI was assumed to depend only on the energy balance arising from minima in the interaction energy profile and Brownian diffusion.^{41,42} The distribution of kinetic energies of diffusing colloids was described by the Maxwellian probability density function. In this case, the Maxwellian cumulative density function was evaluated over specific ranges in the interaction energy profile to determine the probability of colloid interaction (ϵ) with the primary and secondary minima at a particular A_z .^{41,42}

Table 1. Lower (A) and Upper (B) Integration Limits on Equation 3 To Determine ϵ_1 , ϵ_2 , ϵ_{d1} , and ϵ_{d2} for the Five Different Interaction Energy Profile Classes^a

class no.	ϵ_1 A	ϵ_1 B	ϵ_2 A	ϵ_2 B	ϵ_{d1} A	ϵ_{d1} B	ϵ_{d2} A	ϵ_{d2} B
1	0	$ \Phi_{1\min} $	NA	NA	$ \Phi_{1\min} $	∞	NA	NA
2	$ \Phi_{2\min} - \Phi_{\max} $	$ \Phi_{1\min} - \Phi_{\max} $	0	$ \Phi_{2\min} - \Phi_{\max} $	$ \Phi_{1\min} - \Phi_{\max} $	∞	$ \Phi_{2\min} $	∞
3	$ \Phi_{2\min} + \Phi_{\max}$	$ \Phi_{1\min} + \Phi_{\max}$	0	$ \Phi_{2\min} $	$ \Phi_{1\min} + \Phi_{\max}$	∞	$ \Phi_{2\min} $	∞
4	$ \Phi_{2\min} + \Phi_{\max}$	$\Phi_{\max} - \Phi_{1\min}$	0	$ \Phi_{2\min} $	$\Phi_{\max} - \Phi_{1\min}$	∞	$ \Phi_{2\min} $	∞
5	NA	NA	0	$ \Phi_{2\min} $	NA	NA	$ \Phi_{2\min} $	∞

^aNote that ϵ_1 and ϵ_2 equal zero if B < A.

$$\begin{aligned} \epsilon_j &= \int_A^B \frac{2\sqrt{\Phi}}{\sqrt{\pi}} \exp(-\Phi) d\Phi \\ &= \left(\operatorname{erf}(\sqrt{B}) - \sqrt{\frac{4B}{\pi}} \exp(-B) \right) \\ &\quad - \left(\operatorname{erf}(\sqrt{A}) - \sqrt{\frac{4A}{\pi}} \exp(-A) \right) \end{aligned} \quad (3)$$

where A is the lower integration limit, B is the upper integration limit, and the subscript j on ϵ indicates whether the interaction was associated with the primary or secondary minimum ($j = 1$ or 2). Note that eq 3 has been previously employed to estimate ϵ_1 and ϵ_2 on chemically homogeneous^{41,42} and heterogeneous²⁶ surfaces that were assumed to be smooth and had an infinite depth of primary minimum. In contrast, Born repulsion and nanoscale roughness produce a finite depth of primary minimum that allow colloids to sometimes escape the minimum. This was accounted for in eq 3 by selecting values of A and B based on the interaction energy to enter and escape from the minimum, respectively, for the five profile classes. This information is summarized in Table 1.

Colloids interacting with a primary or secondary minimum continue to experience random fluctuations in kinetic energy because of diffusion. Eventually, the colloids will experience the full range of possible kinetic energies; therefore, the probability of detachment from primary (ϵ_{d1}) and secondary (ϵ_{d2}) minima can also be determined using eq 3. Table 1 provides values of ϵ_{d1} and ϵ_{d2} for the five interaction energy profile classes shown in Figure S2. In this case, A reflects the interaction energy to escape the minimum, whereas B is the maximum possible energy. Figure S3 presents a plot of ϵ_{dj} as a function of A. It is evident that the probability of diffusive release rapidly decreases with increasing A and approaches zero when $A > 8k_B T_K$ where k_B and T_K are the Boltzmann constant and the absolute temperature, respectively.

Long-term immobilization at a particular A_z under steady-state conditions of flow and solution chemistry depends on values of ϵ_1 , ϵ_2 , ϵ_{d1} , and ϵ_{d2} . If ϵ_j and ϵ_{dj} are above or below some critical threshold (ϵ_c), respectively, then long-term immobilization is possible. These criteria are expressed mathematically using β_j terms that are given below

$$\beta_1 = H_0(\epsilon_1 - \epsilon_c)H_0(\epsilon_c - \epsilon_{d1}) \quad (4)$$

$$\beta_2 = H_0(\epsilon_2 - \epsilon_c)H_0(\epsilon_c - \epsilon_{d2}) \quad (5)$$

where H_0 is a Heaviside function. The value of $H_0 = 1$ when the quantity in parentheses is greater than or equal to 0, and $H_0 = 0$ when this quantity is less than 0. In this work, we assume a conservative estimate of $\epsilon_c = 0.001$ that allows for diffusive release when the magnitude of the energy barrier to escape the minimum was less than $8k_B T_K$ (cf. Figure S3).

Torque Balance. In the presence of water flow, the balance of applied hydrodynamic and resisting adhesive torques also determines conditions for colloid retention and release at a particular A_z .^{51,52} The hydrodynamic and adhesive torques vary spatially in a porous medium because of the pore-space geometry and grain size distribution, roughness (micro- and nanoscale), and chemical heterogeneity.^{51,52} A torque balance was conducted for each A_z location on the SWI to

determine the influence of adhesive and hydrodynamic conditions on colloid immobilization. Section S2 in the Supporting Information provides full details about the parameter values used in the torque balance calculations. A brief description follows below.

Primary and secondary minima in the interaction energy induce an adhesive force and a resisting adhesive torque that act in the direction opposite to the water flow.^{38,52} The resisting adhesive torque (T_A , ML^2T^{-2}) was determined as²⁷

$$T_A = l_{AP}F_{AP} + l_{AT}F_{AT} \approx l_{AP} \frac{|\Phi_{\min}|}{h_{\min}} + l_{AT} \frac{\Delta\Phi_{\min}}{d_z} \quad (6)$$

where F_{AP} [MLT^{-2}] is the perpendicular component of the adhesive force, F_{AT} [MLT^{-2}] is the tangential component of the adhesive force, l_{AP} [L] is the lever arm associated with F_{AP} , l_{AT} [L] is the lever arm associated with F_{AT} , Φ_{\min} is the interaction energy associated with the minima ($\Phi_{1\min}$ or $\Phi_{2\min}$), h_{\min} [L] is the separation distance for this minimum, and d_z [L] is the diameter of the zone of electrostatic influence.

Water flow produces a drag force and an applied hydrodynamic torque that act on colloids adjacent to a porous medium surface.^{27,43} It also induces a lift force that acts on colloids perpendicular to the solid surface, but this is negligible under laminar flow conditions. The value of the applied hydrodynamic torque (T_H , ML^2T^{-2}) at h_{\min} is determined as⁴³

$$T_H = l_H F_D + M_E = l_H 6\pi\mu_w \tau_w r_c (r_c + h_{\min}) C_h + 4\pi\mu_w \tau_w r_c^3 C_{2h} \quad (7)$$

where τ_w [T^{-1}] is the hydrodynamic shear, μ_w [$ML^{-1}T^{-1}$] is the water viscosity, F_D [MLT^{-2}] is the fluid drag force, l_H [L] is the lever arm associated with F_D , M_E [ML^2T^{-2}] is the moment of external stress, r_c [L] is the colloid radius, and C_h [–] and C_{2h} [–] are dimensionless functions that account for the influence of the SWI. Note that l_{AP} , l_{AT} , and l_H depend on the colloid radius and deformation and the difference in the microscopic roughness height between adjacent zones of influence (Δh_m^*).^{27,37,43} Figure S4 provides a schematic of the influence of microscopic roughness and nanoscale heterogeneity on the lever arms that are used for the torque balance calculations.

Positive values of T_A act in the opposite direction as T_H to decelerate and/or to immobilize colloids ($T_H \leq T_A$), whereas rolling occurs when T_H is greater than T_A . A parameter γ was defined for each A_z to be 1 when $T_H \leq T_A$ and 0 when $T_H > T_A$. Previous literature has focused on the determination of γ for colloids interacting in a secondary minimum.^{27,53} In this work, we determine values of γ_1 and γ_2 to identify locations where colloid immobilization in primary and secondary minima was possible, respectively. Values of γ_1 for a finite depth of a primary minimum provide critical information on the reversibility of interactions on heterogeneous surfaces in the presence of water flow.

Determination of α and S_f within A_z . The above information indicates that values of ϵ_j , ϵ_{dj} , β_j , and γ_j account for the influence of adhesion, diffusion, and hydrodynamics on colloid retention and release for each A_z on the SWI. The probability for colloid immobilization in primary and secondary minima was determined as $\alpha_1 = \epsilon_1 \gamma_1$ and $\alpha_2 = \epsilon_2 \gamma_2$, respectively.^{27,54} To account for the influence of these same factors on colloid release, values of $\alpha_{dj} = \epsilon_{dj}$ if $\gamma_j = 1$ and $\alpha_{dj} = 1$ if $\gamma_j = 0$ were used. The long-term colloid immobilization in

primary and secondary minima was determined as $S_{f1} = \beta_1\gamma_1$ and $S_{f2} = \beta_2\gamma_2$, respectively. If the values of S_{f1} and S_{f2} are both equal to 1 for a particular A_z , then $S_{f1} = 0$ if $\varepsilon_1 < \varepsilon_2$; otherwise, $S_{f2} = 0$.

Upscaled Parameters. The above information indicates that knowledge of the distributions of h_r^m , f_r , ζ_+ , f_+ , h_r^m and the pore-scale water velocity on the SWI is needed to determine colloid retention and release at the REV scale. Accurate determination of these parameter distributions is difficult, if not impossible, for natural systems. Below, we discuss simplified representations of these distributions that can be used to investigate the relative importance of specific factors on colloid retention and release and to show expected trends in parameters with various physicochemical conditions.

The pore-scale water velocity that acts on a colloid adjacent to the SWI (v) varies spatially in a porous medium due to differences in the pore-space geometry.³⁸ Bradford et al.³⁸ conducted pore-scale water flow simulations in idealized sphere packs (colloid transport was not simulated). These authors developed scaling procedures to predict the mean value of the log-normal-distributed v that acts on a given sized colloid adjacent to the solid surface from the average pore water velocity and the median grain size. The probability density function (PDF) for the log-normal distribution is given as⁵⁵

$$\text{PDF}(v) = \frac{1}{\ln(v)\sigma_{\ln(v)}\sqrt{2\pi}} \exp\left[-\frac{(\ln(v) - \mu_{\ln(v)})^2}{2\sigma_{\ln(v)}^2}\right] \quad (8)$$

where $\sigma_{\ln(v)}$ and $\mu_{\ln(v)}$ are the standard deviation and the mean value of the log-normal probability density function, respectively. The value of $\mu_{\ln(v)} = \ln(\langle v \rangle) - 0.5\sigma_{\ln(v)}^2$, where $\langle v \rangle$ is the ensemble average v . The inverse PDF for v was repeatedly sampled in a random manner to encompass the expected range in v over the REV. Figure S5a presents an example distribution of v as a function of number of A_z locations when the colloid size (d_c) = 1000 nm, the median grain size of the porous medium = 360 μm , and the Darcy velocity (q_w) = 0.1 cm min^{-1} .

The lever arms associated with applied hydrodynamic and resisting adhesive torques depend on the value of h_r^m at adjacent A_z locations (Figure S4). A single value of h_r^m was associated with each A_z by randomly sampling a uniform distribution ranging between 0 and 5000 nm. Figure S5b presents an example distribution of h_r^m as a function of number of A_z locations. Grain–grain contacts influence the lever arms for applied and resisting torques in a similar manner as that of microscopic roughness.²⁷ The influence of grain–grain contacts was, therefore, considered to be lumped within this h_r^m distribution.

The simplest form of nanoscale heterogeneity considers binary roughness (0 and h_r^m) and chemical heterogeneity (ζ_- and ζ_+) within each A_z on the SWI. In this case, A_z was divided into a number of equally sized cells with a cross-sectional area of A_h [L^2]. The total number of cells (N_t) within A_z is equal to the rounded value of A_z/A_h ; therefore, $f_r = N_r/N_t$ and $f_+ = N_+/N_t$, where N_r and N_+ are the number of cells within A_z with height h_r^m and zeta potential ζ_+ , respectively. We assumed that nanoscale roughness and chemical heterogeneity are randomly and independently distributed on the SWI. The binomial PDFs for N_r and N_+ are, therefore, described as³⁹

$$\text{PDF}(N_r) = \frac{N_t!}{N_r!(N_t - N_r)!} (P_r)^{N_r} (1 - P_r)^{N_t - N_r} \quad (9)$$

$$\text{PDF}(N_+) = \frac{N_t!}{N_+!(N_t - N_+)!} (P_+)^{N_+} (1 - P_+)^{N_t - N_+} \quad (10)$$

where P_r and P_+ are the total fraction of cells at the REV scale that are occupied by h_r^m and ζ_+ , respectively. The inverse PDFs for N_r and N_+ were repeatedly sampled in a random manner to encompass the expected range in f_r and f_+ on the SWI at the REV scale. It should be mentioned that a number of other PDFs (normal, log-normal, bimodal, etc.) could have been used to describe f_r and f_+ . However, the statistical properties of PDFs change with the size of A_z . In geostatistics, a similar problem occurs with the change in support scale.⁵⁵ An important advantage of the binomial PDF (eqs 9 and 10) is that the statistical properties change in a deterministic way with $N_t =$

A_z/A_h , so the issue of change in support is automatically addressed. For example, the mean and variance of eq 9 are given as $N_r P_r$ and $N_r P_r (1 - P_r)$, respectively.

Natural porous media are expected to exhibit much more complex distributions of nanoscale roughness and chemical heterogeneity than binary heterogeneity. Additional assumptions have to be invoked to achieve greater, more realistic, amounts of nanoscale heterogeneity on the SWI. Consistent with eqs 1 and 2, we continue to assume binary nanoscale heterogeneity within each A_z by using constant values of h_r^m , ζ_+ , and A_h at a given location. However, values of these parameters were now allowed to randomly vary from one A_z to another across the SWI. Values of h_r^m , ζ_+ , and/or A_h for a particular A_z were determined by randomly sampling uniform distributions over a selected range. The mean and variance of the binomial PDFs for N_r and N_+ were unaffected by changes in h_r^m and ζ_+ across the SWI. In contrast, when A_h fluctuated across the SWI, the value of $N_t = A_z/A_h$ in eqs 9 and 10 also changed with each A_z location. This implies that the PDF at the REV scale is the superposition of a number (determined by the range in A_h) of binomial PDFs with different values of N_t and the same value of P_r or P_+ . Figure S5c,d presents example distributions of input parameters of f_r and f_+ , respectively, as a function of number of A_z locations when the solution IS = 10 mM NaCl, $d_c = 1000$ nm, $P_+ = 0.05$, $P_r = 0.1$, $A_h = 100\text{--}1000$ nm^2 for nanoscale chemical heterogeneity, and $A_h = 100$ nm^2 to A_z for nanoscale roughness.

Values of α_1 , α_2 , α_{d1} , α_{d2} , S_{f1} , and S_{f2} were calculated for each A_z on the SWI using the approach outlined in the previous section. On the basis of results of a sensitivity analysis shown in Figure S6, upscaled values of α_1 , α_2 , α_{d1} , α_{d2} , S_{f1} , and S_{f2} were determined as the average value of greater than 999 A_z realizations (described above). The variance in these same parameters was also calculated. For example, the variance of α_1 is given as $\langle \alpha_1^2 \rangle - \langle \alpha_1 \rangle^2$, and the associated standard deviation is equal to the square root of the variance. The total values of $\alpha = \alpha_1 + \alpha_2$ and $S_f = S_{f1} + S_{f2}$. The above calculations were implemented into Microsoft Excel using Visual Basics for Applications programming language.

RESULTS AND DISCUSSION

Simulations discussed below considered extended DLVO interactions, energy balance, and torque balance calculations for a homogeneous colloid interacting with a heterogeneous porous medium surface at more than 999 locations. Values of water velocity in the vicinity of the solid surface were spatially distributed to be consistent with a porous medium having a median grain size of 360 μm and a selected q_w . A constant IS was considered for each simulation. Separate regression equations were used to predict the zeta potentials for the homogeneous colloid and the negative portion of solid surface as a function of IS. These equations were derived from experimental zeta potential measurements presented by Treumann et al.²⁰ for carboxyl-modified latex microspheres and ultrapure quartz sand. Other extended-DLVO and torque balance parameters were taken to be consistent with latex microspheres, including the Hamaker constant = 4.04×10^{-21} J, collision diameter = 0.25 nm, characteristic wavelength = 100 nm, and the composite Young's modulus = 4.01×10^9 N m^{-2} .

The outlined modeling approach has the ability to examine the influence of specific factors, individually or in combination, on colloid retention and release. Specific simulations were conducted to investigate the influence of the following factors on upscaled colloid retention parameters: (i) nanoscale chemically heterogeneity (denoted CH) on a smooth SWI, (ii) nanoscale roughness (denoted NR) on a chemically homogeneous SWI, (iii) the combination of NR + CH on the SWI, and (iv) the combination of microscopic roughness (MR), NR, and CH (denoted MR + NR + CH) on the SWI. When CH was considered, a constant value of P_+ was selected,

$A_h = 100\text{--}1000\text{ nm}^2$, and $\zeta_+ = 0\text{--}30\text{ mV}$. When NR was considered, a constant value of P_r was selected, $A_h = 100\text{ nm}^2$ to A_z , and $h_r^m = 0\text{--}50\text{ nm}$. When MR was considered, $h_r^m = 0\text{--}5000\text{ nm}$. Below, we present representative simulations to show that our modeling approach can be utilized to obtain insight on mechanisms for colloid retention and release under each of these situations.

Chemical Heterogeneity. Figure 1 presents the influence of P_+ (0.025, 0.05, 0.1, and 0.2) on simulated values of $\alpha = \alpha_1 +$

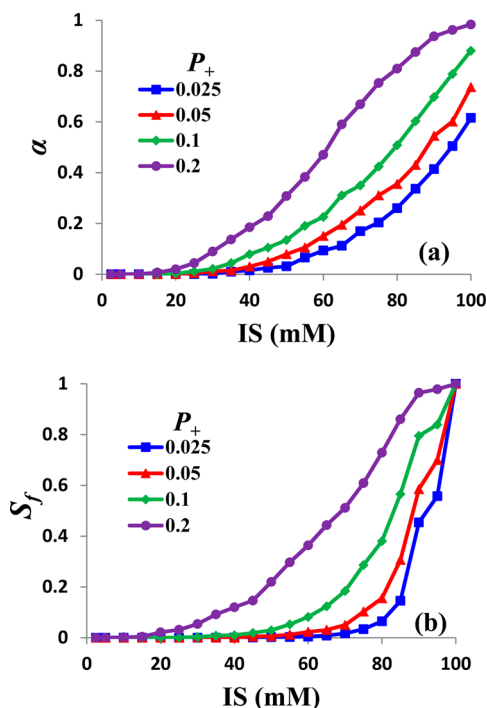


Figure 1. Mean values of α and S_f for various values of P_+ (0.025, 0.05, 0.1, and 0.2) for a 1000 nm colloid as a function of IS (1–100 mM NaCl) when $q_w = 0.1\text{ cm min}^{-1}$. Individual simulation results from the CH model are indicated with a data point. The trend lines that connect the data points are intended only to guide the eye of the reader.

α_2 (Figure 1a) and $S_f = S_{f1} + S_{f2}$ (Figure 1b) for a 1000 nm colloid as a function of IS (1–100 mM NaCl) when $q_w = 0.1\text{ cm min}^{-1}$. It is interesting to note that a negligible fraction of the solid surface was available for retention (i.e., very low α and S_f values) when the IS < 20 mM, even when the value of P_+ was 0.2 (i.e., the overall probability of nanoscale positive charges on the SWI was 20%). Further increase in the IS produced an increase in α and S_f , indicating that more localized sites became available for colloid retention, especially for increasing P_+ . This result is consistent with published literature reporting that α and S_f increased with P_+ , A_h , and ζ_+ .^{26,56} Note that wide distributions of A_h and ζ_+ were considered in the simulations shown in Figure 1. The values of α and S_f were relatively similar at any given IS and P_+ because colloids interacted with deep primary minima on the smooth SWI.³⁹ This result is consistent with the assumption of filtration theory that colloid retention on the SWI is largely irreversible. As expected, the entire solid surface contributed to colloid retention (i.e., $S_f = 1$) when the energy barrier was eliminated as the IS approached 100 mM.

Figure 2 presents the influence of q_w (0.001, 0.01, 0.1, 1, and 10 cm min^{-1}) on values of $\alpha = \alpha_1 + \alpha_2$ (Figure 2a) and $S_f = S_{f1} + S_{f2}$ (Figure 2b) for a 1000 nm colloid as a function of IS (1–

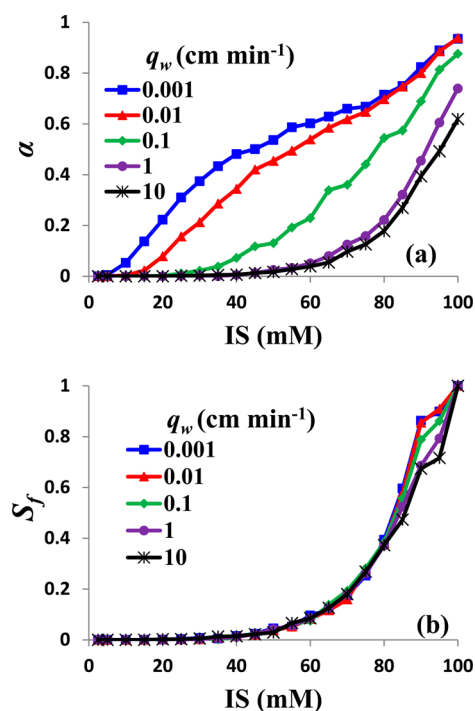


Figure 2. Mean values of α and S_f for a 1000 nm colloid for various q_w (0.001, 0.01, 0.1, 1, and 10 cm min^{-1}) and IS (1–100 mM NaCl) when $P_+ = 0.05$. Individual simulation results from the CH model are indicated with a data point. The trend lines that connect the data points are intended only to guide the eye of the reader.

100 mM NaCl) when $P_+ = 0.05$. Figure 2b shows that the value of S_f was largely independent of q_w because long-term colloid retention occurred in deep primary energy minima. Indeed, values of S_f and α_1 were nearly identical (data not shown), and α_1 would, therefore, provide an estimate for the irreversible colloid sticking efficiency. In contrast to S_f , the total value of α ($\alpha_1 + \alpha_2$) was strongly dependent on q_w , suggesting that a large fraction of colloids interacted in secondary energy minima. In particular, the value of α tended to become much larger than S_f as q_w decreased because the torque balance was satisfied at low flow velocities, but Brownian forces prevented long-term retention in most secondary minima.

Nanoscale Roughness. Figure 3 presents the influence of q_w (0.001, 0.01, 0.1, 1, and 10 cm min^{-1}) on values of α_1 (Figure 3a), α_2 (Figure 3b), and S_f (Figure 3c) for a 1000 nm colloid as a function of IS (1–100 mM NaCl) when $P_r = 0.1$. In contrast to the chemical heterogeneity simulations, values of α_1 and α_2 both decreased with increasing q_w in the presence of nanoscale roughness. This implies that both secondary and primary minimum interactions were subject to hydrodynamic release. Conversely, the value of S_f was largely independent of q_w , and this indicates that only deep energy minima contributed to long-term colloid retention.

Figure 4 presents the influence of P_r (0.025, 0.05, 0.1, 0.2, and 0.4) on values of α_1 (Figure 4a), α_2 (Figure 4b), and S_f (Figure 4c) for a 1000 nm colloid as a function of IS (1–100 mM NaCl) when $q_w = 0.1\text{ cm min}^{-1}$. A decrease in P_r produced an increase in α_1 (Figure 4a) and a decrease in α_2 (Figure 4b). Similarly, the literature has reported that decreasing P_r results in a reduction of the energy barrier, more primary minimum interactions, and a weaker secondary minimum.^{33–36,39,40} The total value of $\alpha = \alpha_1 + \alpha_2$ (cf. Figure 4a,b) increased with IS, but it was relatively insensitive to P_r . The dependence of S_f on

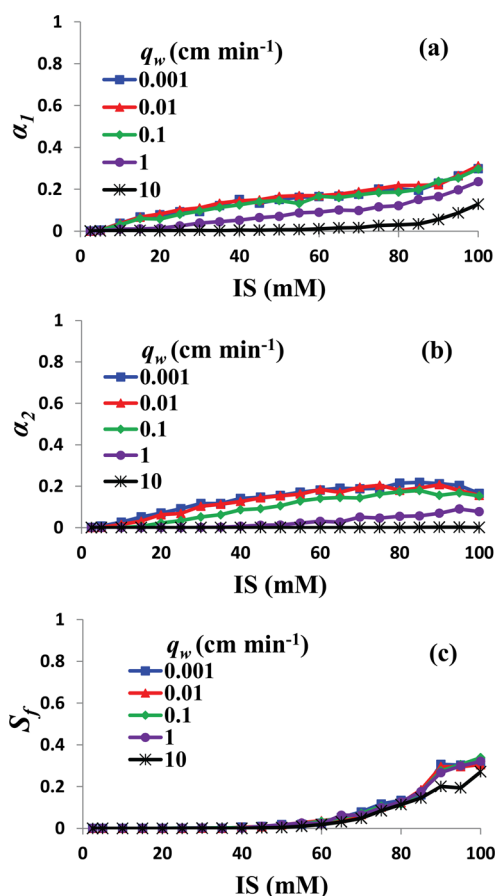


Figure 3. Mean values of α_1 , α_2 , and S_f for a 1000 nm colloid for various q_w (0.001, 0.01, 0.1, 1, and 10 cm min^{-1}) and IS (1–100 mM NaCl) when $P_r = 0.1$. Individual simulation results from the NR model are indicated with a data point. The trend lines that connect the data points are intended only to guide the eye of the reader.

nanoscale roughness was complex due to differences in the functionality of van der Waals and electrostatic interactions with separation distance. The value of S_f was practically zero when the IS was less than or equal to 20 mM, even though shallow primary minimum interactions occurred under these conditions (Figure 4a). Primary minimum interactions were stronger and more frequent when the IS ranged from around 20 to 50 mM (Figure 4a), especially when P_r was 0.025 and 0.05, and this produced low values of S_f . The value of S_f tended to increase with IS and P_r when the IS ranged from 50 to 100 mM because both primary and secondary minima became deeper. However, values of α and S_f were still much less than 1 even when the IS was as high as 100 mM. Indeed, experimental values of S_f have also been reported to be very small, even when the IS > 100 mM.^{18–20,57,58} These findings support the importance of nanoscale roughness in producing weak primary minimum interactions that limit colloid retention and promote release under high IS conditions.

Similar to the chemical heterogeneity simulations, the value of S_f in Figures 3c and 4c was mainly controlled by primary minimum interactions, and the secondary minimum did not contribute to long-term retention until the IS was greater than 80 mM. In contrast, the value of S_f was considerably lower than α at a given IS. Similarly, experimental values of S_f have sometimes been observed to be much lower than α .^{57,58} This result implies that both primary and secondary minima

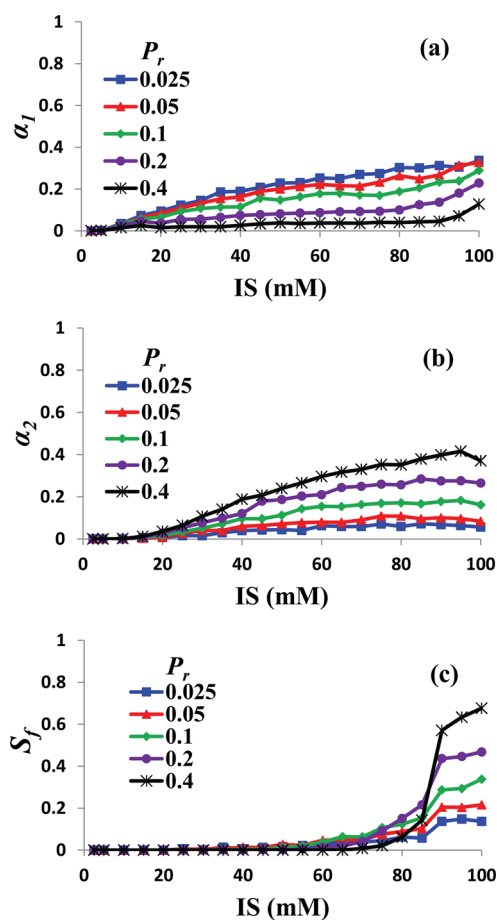


Figure 4. Mean values of α_1 , α_2 , and S_f for a 1000 nm colloid for various P_r (0.025, 0.05, 0.1, 0.2, and 0.4) and IS (1–100 mM NaCl) when $q_w = 0.1 \text{ cm min}^{-1}$. Individual simulation results from the NR model are indicated with a data point. The trend lines that connect the data points are intended only to guide the eye of the reader.

interactions were relatively weak on a surface containing nanoscale roughness and that most retained colloids were subject to diffusive release. This occurs because nanoscale roughness substantially reduces the depth of the primary minimum compared to that of smooth surfaces.^{39,40} Mean-field DLVO calculations and the CFT assumption of irreversible colloid retention are, therefore, unlikely to be valid on natural surfaces that always exhibit nanoscale roughness. An estimate for irreversible values of α_1 and α_2 for each A_z location could have been obtained as $\epsilon_1 \gamma_1 H_0(\epsilon_c - \epsilon_{d1})$ and $\epsilon_2 \gamma_2 H_0(\epsilon_c - \epsilon_{d2})$, respectively. This alternative approach would have allowed only locations with minima deeper than $8k_B T_K$ ($\epsilon_c = 0.001$) to contribute to both α and S_b but it would not have revealed the significant influence of reversible retention processes on α . Calculated values α_{d1} and α_{d2} are expected to be of critical importance in determining kinetic rates of colloid release, but they were not the focus of this study.

Nanoscale Roughness and Chemical Heterogeneity.

Figure 5 compares simulated values of α (Figure 5a) and S_f (Figure 5b) among the CH, NR, and NR + CH models when $P_r = 0.1$, $P_+ = 0.05$, the IS ranged from 1 to 100 mM NaCl, and $q_w = 0.1 \text{ cm min}^{-1}$. Values of S_f in Figure 5b are plotted on a log-scale. Figure 5 clearly reveals the relative importance of nanoscale chemical heterogeneity and nanoscale roughness on colloid retention. Results were quite similar between the NR

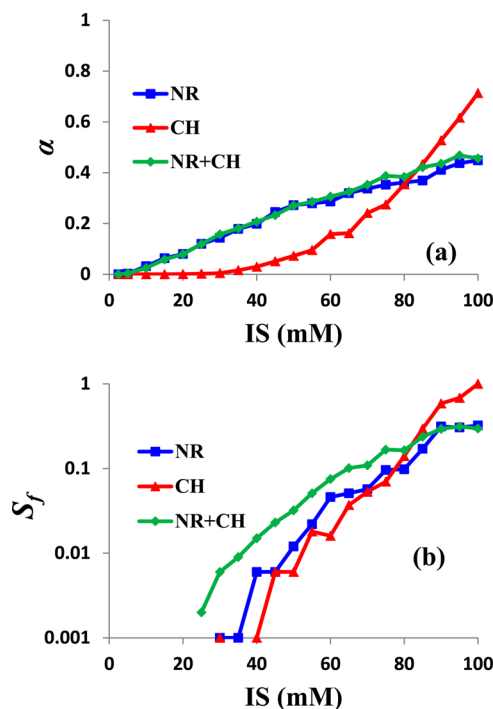


Figure 5. Mean values of α and S_f for a 1000 nm colloid for various IS (1–100 mM NaCl), $q_w = 0.1 \text{ cm min}^{-1}$, when using the CH ($P_+ = 0.05$), NR ($P_r = 0.1$), and NR + CH ($P_+ = 0.05$ and $P_r = 0.1$) models. Values of S_f in (b) are plotted on a log-scale so that differences in the simulation results are more apparent. Individual simulation results are indicated with a data point. The trend lines that connect the data points are intended only to guide the eye of the reader.

and NR + CH models. This finding indicates that NR mainly control the colloid interaction energies on natural surfaces, even in the presence of a significant fraction of CH. When IS < 80 mM, the combined NR + CH simulation provided higher values of S_f than the NR model and especially the CH model because CH and NR lowered the energy barrier to a greater extent and produced more primary minimum interactions.^{35,39} Conversely, when IS \geq 80 mM, the values of α and S_f for the NR + CH model were dramatically reduced relative to those for the CH model because NR reduced the energy to escape from the primary minimum.^{39,40} This allowed for more colloid to be released by hydrodynamic and diffusive forces.⁴⁰ A similar dependence of α on q_w was, therefore, observed for the surfaces containing NR + CH and NR (see Figure 3a,b for the NR model).

Microscopic Roughness. Simulations shown in Figures 1–5 accounted only for the influence of CH and/or NR on colloid attachment. Surface straining processes also contribute to colloid retention at MR locations. In particular, MR facilitates colloid retention by lowering the lever arm for the applied hydrodynamic torque and increasing the lever arm for the resisting adhesive torque.^{27,37} The fraction that MR contributes to α (f_{MR}) can be calculated as $f_{MR} = (\alpha(\text{MR} + \text{NR} + \text{CH}) - \alpha(\text{NR} + \text{CH})) / \alpha(\text{MR} + \text{NR} + \text{CH})$, where $\alpha(\text{MR} + \text{NR} + \text{CH})$ and $\alpha(\text{NR} + \text{CH})$ are simulated values of α when MR + NR + CH and NR + CH were considered on the SWI, respectively. Figure 6a presents values of f_{MR} for various q_w when the IS ranged from 1 to 100 mM NaCl, $d_c = 1000 \text{ nm}$, $P_r = 0.1$, and $P_+ = 0.05$. Figure 6b presents values of f_{MR} for various d_c when the IS ranged from 1 to 100 mM NaCl, $q_w = 0.1 \text{ cm min}^{-1}$, $P_r = 0.1$, and $P_+ = 0.05$. Note that MR plays a

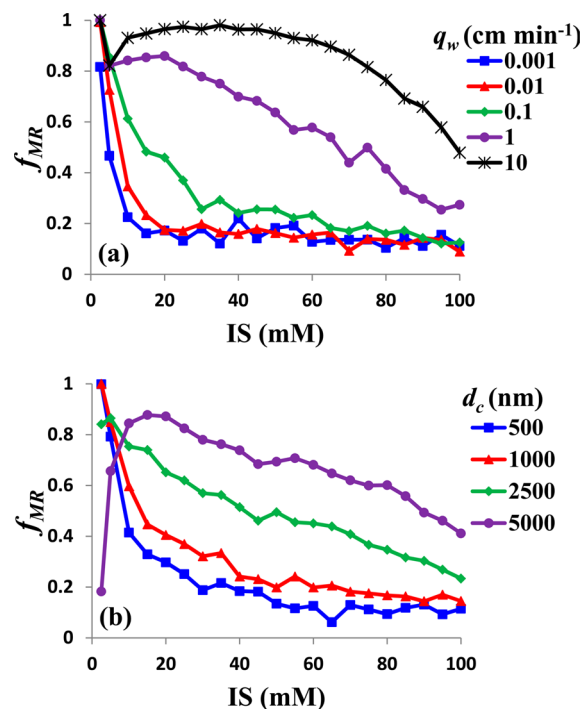


Figure 6. Plots of the fraction of α that is contributed by MR (f_{MR}) as a function of IS (1–100 mM). (a) Values of f_{MR} for various q_w when the $d_c = 1000 \text{ nm}$, $P_r = 0.1$, and $P_+ = 0.05$. (b) Values of f_{MR} for various d_c when $q_w = 0.1 \text{ cm min}^{-1}$, $P_r = 0.1$, and $P_+ = 0.05$. Individual simulation results are indicated with a data point. The trend lines that connect the data points are intended only to guide the eye of the reader.

dominant role in α for higher q_w and d_c (higher hydrodynamic forces) and lower IS (lower adhesive forces). Under these conditions, the torque balance may not be satisfied on a microscopically smooth surface, but it can be at MR locations because of altered lever arms. Experimental observations have demonstrated enhanced colloid retention at MR locations under low IS conditions and for larger colloid sizes.⁵⁹

Figure 6 also indicates that the f_{MR} decreases with lower q_w and d_c (lower hydrodynamic forces) and higher IS (higher adhesive forces). Under these cases, the torque balance may be satisfied on a microscopically smooth surface, and the relative importance of MR on α , therefore, decreases. This implies that the contribution of NR and CH to colloid retention increases with lower q_w and d_c and higher IS. Indeed, colloid retention has been previously reported to be more sensitive to CH and NR for smaller values of d_c and higher IS.^{35,43}

Figures 1–6 and associated discussion can be used to help interpret values of α and S_f for various IS, q_w and d_c conditions. For example, Figure 7 presents values of α from the MR + NR + CH model as a function of IS (1–100 mM) when $P_r = 0.1$, $P_+ = 0.05$, q_w ranges from 0.001 to 10 cm min^{-1} , and d_c equals 1000 nm (Figure 7a) and 5000 nm (Figure 7b). Corresponding values of S_f for these same conditions are given in Figure 8. Note that α and S_f values at a given IS and q_w were higher for larger colloids. Furthermore, α and S_f as a function of IS did not vary much with q_w when $d_c = 1000 \text{ nm}$ (Figures 7a and 8a), whereas both decreased with increasing q_w when $d_c = 5000 \text{ nm}$ (Figures 7b and 8b). These differences reflect the influence of colloid size on the retention process on a physically and chemically heterogeneous surface. As mentioned in discussion associated with Figure 6, the relative importance of MR, NR,

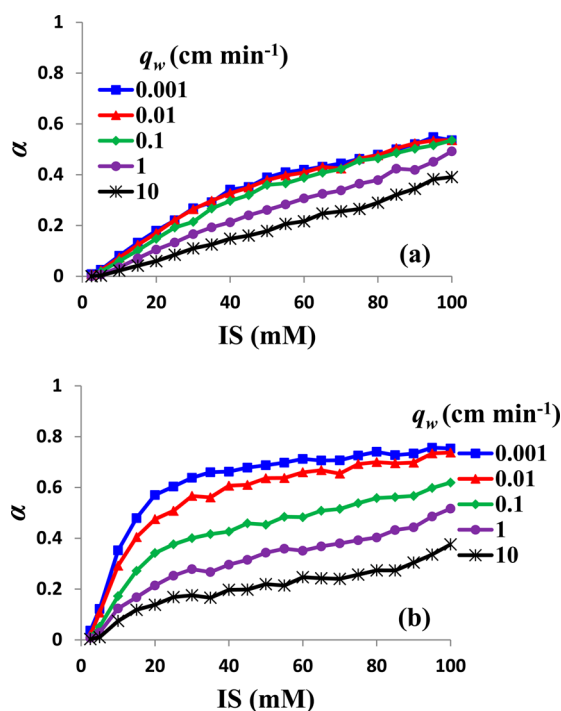


Figure 7. Mean values of α for the MR + NR + CH model ($P_r = 0.1$ and $P_+ = 0.05$) with the indicated values of q_w and IS when $d_c = 1000$ nm (a) and 5000 nm (b). Individual simulation results are indicated with a data point. The trend lines that connect the data points are intended only to guide the eye of the reader.

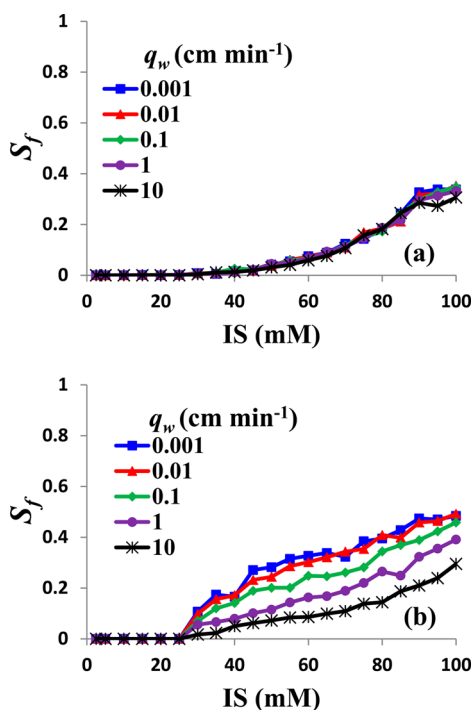


Figure 8. Mean values of S_f for the MR + NR + CH model ($P_r = 0.1$ and $P_+ = 0.05$) with the indicated values of q_w and IS when $d_c = 1000$ nm (a) and 5000 nm (b). Individual simulation results are indicated with a data point. The trend lines that connect the data points are intended only to guide the eye of the reader.

and CH on α changes with the IS, q_w , and d_c conditions. MR controls values of α at lower IS, higher q_w , and higher d_c . In

contrast, NR and CH determine values of α at higher IS, lower q_w , and lower d_c .

In addition, NR and CH always play a critical role in determining the value of S_f because of their strong influence on the depth of the primary and secondary minima, even when MR controls the value of α . Figure 5b indicated that the value of S_f will be mainly controlled by NR parameters, especially at higher IS. However, it is possible that the relative importance of NR and CH on the determination of S_f may change with selected nanoscale roughness (A_h , h_r , and P_r), chemical heterogeneity (A_h , ζ_+ , and P_+), and interaction energy (Hamaker constant, zeta potentials) parameters. Furthermore, the influence of MR on S_f is likely to be underestimated in these calculations because they always allow for diffusive release of colloids when minima were less than $8k_B T_K$ ($\epsilon_c = 0.001$). In reality, diffusive release of colloids at MR locations and grain-grain contacts may be less likely than that on a microscopically smooth surface because of the presence of eddy zones.⁶⁰ This effect could be potentially included in S_f calculations by making ϵ_c a higher value at MR locations. Figure S7 demonstrates the influence of ϵ_c on predicted values of S_f for the MR + NR + CH model as a function of IS when $P_r = 0.1$, $P_+ = 0.05$, $q_w = 0.1$ cm min⁻¹, and $d_c = 1000$ nm (Figure S7a) and 5000 nm (Figure S7b). Note that values of S_f increase with increasing ϵ_c , approaching the value of α (cf. Figure 7). Consequently, the influence of MR on S_f will also increase with ϵ_c .

CONCLUSIONS

Extended DLVO, energy balance, and torque balance calculations for a homogeneous colloid over a heterogeneous porous medium surface provided predictions for upscaled values of retention and release parameters (α_1 , α_2 , α_{d1} , α_{d2} , S_{f1} , and S_{f2}) and insight into mechanisms controlling colloid retention. In particular, values of α and S_f were observed to be frequently controlled by primary minimum interactions even under so-called “unfavorable” conditions because of the influence of nanoscale roughness and/or chemical heterogeneity. However, the value of the primary minimum was shallow on a nanoscale rough surface, and some locations were subject to diffusive and hydrodynamic removal depending on the roughness parameters. The role of the secondary minimum was diminished on the heterogeneous surface because of nanoscale roughness. Microscopic roughness was demonstrated to play a dominant role in colloid retention under low IS conditions and for increased hydrodynamic forces (e.g., higher velocities and larger colloid sizes). However, these effects also depended on the nanoscale roughness parameters at higher IS. The role of chemical heterogeneity was enhanced for larger amounts of chemical heterogeneity and for larger values of A_h/A_z (e.g., small d_c and higher IS). Section S3 in the Supporting Information contains some discussion about future plans to expand and to experimentally validate our modeling framework.

ASSOCIATED CONTENT

Supporting Information

The Supporting Information is available free of charge on the ACS Publications website at DOI: 10.1021/acs.langmuir.5b03080.

Details pertaining to extended-DLVO calculations (Section S1), torque balance calculations (Section S2), and future plans to expand and experimentally validate our modeling framework (Section S3); schematic

illustrating the influence of nanoscale roughness and chemical heterogeneity on interaction energies within A_z (Figure S1); example interaction energy profiles that are representative of five classes found on a heterogeneous SWI (Figure S2); plot of ϵ_{jd} as a function of A (Figure S3); schematic illustrating the influence of microscopic roughness and nanoscale heterogeneity on the lever arms that are used for the torque balance calculations (Figure S4); example plots of input parameters (ν , h_r^m , f_v , and f_+) for simulations (Figure S5); results from a sensitivity analysis for various number of A_z realizations (Figure S6); influence of ϵ_c on predicted values of S_f for the MR + NR + CH model (Figure S7) (PDF)

AUTHOR INFORMATION

Corresponding Author

*Phone: 951-369-4857; E-mail: scott.bradford@ars.usda.gov.

Notes

The authors declare no competing financial interest.

ACKNOWLEDGMENTS

This research was supported by the USDA, ARS, NP 214. The USDA is an equal opportunity provider and employer.

REFERENCES

- (1) Ryan, J. N.; Elimelech, M. Colloid mobilization and transport in groundwater. *Colloids Surf., A* **1996**, *107*, 1–56.
- (2) Khilar, K. C.; Fogler, H. S. *Migrations of Fines in Porous Media*; Kluwer Academic Publishers: Dordrecht, The Netherlands, 1998.
- (3) Harvey, R. W.; Harms, H. Transport of microorganisms in the terrestrial subsurface: In situ and laboratory methods. In *Manual of Environmental Microbiology*; Hurst, C.J., Knudsen, G.R., McInerney, M.J., Stetzenback, L.D., Crawford, R.L., Eds.; ASM Press: Washington, DC, 2002; pp 753–776.
- (4) Foppen, J. W. A.; Schijven, J. F. Evaluation of data from the literature on the transport and survival of *Escherichia coli* and thermotolerant coliforms in aquifers under saturated conditions. *Water Res.* **2006**, *40*, 401–426.
- (5) Sen, T. K.; Khilar, K. C. Review on subsurface colloids and colloid-associated contaminant transport in saturated porous media. *Adv. Colloid Interface Sci.* **2006**, *119*, 71–96.
- (6) Pang, L. Microbial removal rates in subsurface media estimated from published studies of field experiments and large intact soil cores. *J. Environ. Qual.* **2009**, *38*, 1531–1559.
- (7) Schijven, J. K.; Hassanizadeh, S. M. Removal of viruses by soil passage: Overview of modeling, processes, and parameters. *Crit. Rev. Environ. Sci. Technol.* **2000**, *30*, 49–127.
- (8) Molnar, I. L.; Johnson, W. P.; Gerhard, J. I.; Willson, C. S.; O'Carroll, D. M. Predicting colloid transport through saturated porous media: A critical review. *Water Resour. Res.* **2015**, *51*, 6804–6845.
- (9) Ginn, T. R.; Wood, B. D.; Nelson, K. E.; Scheibe, T. D.; Murphy, E. M.; Clement, T. P. Processes in microbial transport in the natural subsurface. *Adv. Water Resour.* **2002**, *25*, 1017–1042.
- (10) Bradford, S. A.; Wang, Y.; Kim, H.; Torkzaban, S.; Simunek, J. Modeling microorganism transport and survival in the subsurface. *J. Environ. Qual.* **2014**, *43*, 421–440.
- (11) Johnson, P. R.; Sun, N.; Elimelech, M. Colloid transport in geochemically heterogeneous porous media: Modeling and measurements. *Environ. Sci. Technol.* **1996**, *30*, 3284–3293.
- (12) Tufenkji, N. Modeling microbial transport in porous media: Traditional approaches and recent developments. *Adv. Water Resour.* **2007**, *30*, 1455–1469.
- (13) Yao, K. M.; Habibiyan, M. T.; O'Melia, C. R. Water and waste water filtration. Concepts and applications. *Environ. Sci. Technol.* **1971**, *5*, 1105–1112.
- (14) Tufenkji, N.; Elimelech, M. Correlation equation for predicting single-collector efficiency in physicochemical filtration in saturated porous media. *Environ. Sci. Technol.* **2004**, *38*, 529–536.
- (15) Leij, F. J.; Bradford, S. A.; Wang, Y.; Sciortino, A. Langmuirian blocking of irreversible colloid retention: Analytical solution, moments, and setback distance. *J. Environ. Qual.* **2015**, *44*, 1473.
- (16) Liang, Y.; Bradford, S. A.; Simunek, J.; Vereecken, H.; Klumpp, E. Sensitivity of the transport and retention of stabilized silver nanoparticles to physicochemical factors. *Water Res.* **2013**, *47*, 2572–2582.
- (17) Liang, Y.; Bradford, S. A.; Simunek, J.; Heggen, M.; Vereecken, H.; Klumpp, E. Retention and remobilization of stabilized silver nanoparticles in an undisturbed loamy sand soil. *Environ. Sci. Technol.* **2013**, *47*, 12229–12237.
- (18) Sasidharan, S.; Torkzaban, S.; Bradford, S. A.; Dillon, P. J.; Cook, P. G. Coupled effects of hydrodynamic and solution chemistry on long-term nanoparticle transport and deposition in saturated porous media. *Colloids Surf., A* **2014**, *457*, 169–179.
- (19) Bradford, S. A.; Kim, H. N.; Haznedaroglu, B. Z.; Torkzaban, S.; Walker, S. L. Coupled factors influencing concentration-dependent colloid transport and retention in saturated porous media. *Environ. Sci. Technol.* **2009**, *43*, 6996–7002.
- (20) Treumann, S.; Torkzaban, S.; Bradford, S. A.; Visalakshan, R. M.; Page, D. An explanation for differences in the process of colloid adsorption in batch and column studies. *J. Contam. Hydrol.* **2014**, *164*, 219–229.
- (21) Elimelech, M. Predicting collision efficiencies of colloidal particles in porous media. *Water Res.* **1992**, *26*, 1–8.
- (22) Bai, R.; Tien, C. A New Correlation for the Initial Filter Coefficient under Unfavorable Surface Interactions. *J. Colloid Interface Sci.* **1996**, *179*, 631–634.
- (23) Bai, R.; Tien, C. Particle Deposition under Unfavorable Surface Interactions. *J. Colloid Interface Sci.* **1999**, *218*, 488–499.
- (24) Chang, Y.-I.; Cheng, W.-Y.; Chan, H.-C. A proposed correlation equation for predicting filter coefficient under unfavorable deposition conditions. *Sep. Purif. Technol.* **2009**, *65*, 248–250.
- (25) Phenrat, T.; Song, J. E.; Cisneros, C. M.; Schoenfelder, D. P.; Tilton, R. D.; Lowry, G. V. Estimating Attachment of Nano- and Submicrometer-particles Coated with Organic Macromolecules in Porous Media: Development of an Empirical Model. *Environ. Sci. Technol.* **2010**, *44*, 4531–4538.
- (26) Bradford, S. A.; Torkzaban, S. Colloid adhesive parameters for chemically heterogeneous porous media. *Langmuir* **2012**, *28*, 13643–13651.
- (27) Bradford, S. A.; Torkzaban, S.; Shapiro, A. A theoretical analysis of colloid attachment and straining in chemically heterogeneous porous media. *Langmuir* **2013**, *29*, 6944–6952.
- (28) Pazmino, E. F.; Trauscht, J.; Johnson, W. P. Release of colloids from primary minimum contact under unfavorable conditions by perturbations in ionic strength and flow rate. *Environ. Sci. Technol.* **2014**, *48*, 9227–9235.
- (29) Pazmino, E. F.; Trauscht, J.; Dame, B.; Johnson, W. P. Power law size-distributed heterogeneity explains colloid retention on soda lime glass in the presence of energy barriers. *Langmuir* **2014**, *30*, 5412–5421.
- (30) Bendersky, M.; Santore, M. M.; Davis, J. M. Statistically-based DLVO approach to the dynamic interaction of colloidal microparticles with topographically and chemically heterogeneous collectors. *J. Colloid Interface Sci.* **2015**, *449*, 443–451.
- (31) Vaidyanathan, R.; Tien, C. Hydrosol deposition in granular media under unfavorable surface conditions. *Chem. Eng. Sci.* **1991**, *46*, 967–983.
- (32) Tufenkji, N.; Elimelech, M. Breakdown of colloid filtration theory: Role of the secondary energy minimum and surface charge heterogeneities. *Langmuir* **2005**, *21*, 841–852.
- (33) Hoek, E. M. V.; Bhattacharjee, S.; Elimelech, M. Effect of membrane surface roughness on colloid-membrane DLVO interactions. *Langmuir* **2003**, *19*, 4836–4847.

- (34) Huang, X.; Bhattacharjee, S.; Hoek, E. M. V. Is surface roughness a “scapegoat” or a primary factor when defining particle-substrate interactions? *Langmuir* **2010**, *26*, 2528–2537.
- (35) Bendersky, M.; Davis, J. M. DLVO interaction of colloidal particles with topographically and chemically heterogeneous surfaces. *J. Colloid Interface Sci.* **2011**, *353*, 87–97.
- (36) Suresh, L.; Walz, J. Y. Effect of surface roughness on the interaction energy between a colloidal sphere and a flat plate. *J. Colloid Interface Sci.* **1996**, *183*, 199–213.
- (37) Burdick, G. M.; Berman, N. S.; Beaudoin, S. P. Hydrodynamic particle removal from surfaces. *Thin Solid Films* **2005**, *488*, 116–123.
- (38) Bradford, S. A.; Torkzaban, S.; Wiegmann, A. Pore-scale simulations to determine the applied hydrodynamic torque and colloid immobilization. *Vadose Zone J.* **2011**, *10*, 252–261.
- (39) Bradford, S. A.; Torkzaban, S. Colloid interaction energies for physically and chemically heterogeneous porous media. *Langmuir* **2013**, *29*, 3668–3676.
- (40) Shen, C.; Lazouskaya, V.; Jin, Y.; Li, B.; Ma, Z.; Zheng, W.; Huang, Y. Coupled factors influencing detachment of nano- and micro-sized particles from primary minima. *J. Contam. Hydrol.* **2012**, *134–135*, 1–11.
- (41) Simoni, S. F.; Harms, H.; Bosma, T. N. P.; Zehnder, A. J. B. Population heterogeneity affects transport of bacteria through sand columns at low flow rates. *Environ. Sci. Technol.* **1998**, *32*, 2100–2105.
- (42) Shen, C.; Li, B.; Huang, Y.; Jin, Y. Kinetics of coupled primary- and secondary-minimum deposition of colloids under unfavorable chemical conditions. *Environ. Sci. Technol.* **2007**, *41*, 6976–6982.
- (43) Duffadar, R. D.; Davis, J. M. Dynamic adhesion behavior of micrometer-scale particles flowing over patchy surfaces with nanoscale electrostatic heterogeneity. *J. Colloid Interface Sci.* **2008**, *326*, 18–27.
- (44) Derjaguin, B. V.; Landau, L. D. Theory of the stability of strongly charged lyophobic sols and of the adhesion of strongly charged particles in solutions of electrolytes. *Acta Physicochim. U.S.S.R.* **1941**, *14*, 733–762.
- (45) Verwey, E. J. W.; Overbeek, J. Th. G. *Theory of the Stability of Lyophobic Colloids*; Elsevier: Amsterdam, 1948.
- (46) Israelachvili, J. N. *Intermolecular and Surface Forces*; Academic Press: San Diego, CA, 1992.
- (47) Elimelech, M.; Gregory, J.; Jia, X.; Williams, R. A. *Particle Deposition and Aggregation: Measurement, Modeling, and Simulation*; Butterworth-Heinemann: Oxford, England, 1995.
- (48) Hogg, R.; Healy, T. W.; Fuerstenau, D. W. Mutual coagulation of colloidal dispersions. *Trans. Faraday Soc.* **1966**, *62*, 1638–1651.
- (49) Gregory, J. Approximate expression for retarded van der Waals interaction. *J. Colloid Interface Sci.* **1981**, *83*, 138–145.
- (50) Ruckenstein, E.; Prieve, D. C. Adsorption and desorption of particles and their chromatographic separation. *AIChE J.* **1976**, *22*, 276–285.
- (51) Bergendahl, J.; Grasso, D. Colloid generation during batch leaching tests: mechanics of disaggregation. *Colloids Surf, A* **1998**, *135*, 193–205.
- (52) Bergendahl, J.; Grasso, D. Prediction of colloid detachment in a model porous media: hydrodynamics. *Chem. Eng. Sci.* **2000**, *55*, 1523–1532.
- (53) Torkzaban, S.; Bradford, S. A.; Walker, S. L. Resolving the coupled effects of hydrodynamics and DLVO forces on colloid attachment to porous media. *Langmuir* **2007**, *23*, 9652–9660.
- (54) Shen, C.; Huang, Y.; Li, B.; Jin, Y. Predicting attachment efficiency of colloid deposition under unfavorable attachment conditions. *Water Resour. Res.* **2010**, *46*, W11526.
- (55) Isaaks, E. H.; Srivastava, R. M. *An Introduction to Applied Geostatistics*; Oxford University Press: New York, 1989.
- (56) Elimelech, M.; Nagai, M.; Ko, C. H.; Ryan, J. N. Relative insignificance of mineral grain zeta potential to colloid transport in geochemically heterogeneous porous media. *Environ. Sci. Technol.* **2000**, *34*, 2143–2148.
- (57) Wang, Y.; Li, Y.; Fortner, J. D.; Hughes, J. B.; Abriola, L. M.; Pennell, K. D. Transport and retention of nanoscale C60 aggregates in water-saturated porous media. *Environ. Sci. Technol.* **2008**, *42*, 3588–3594.
- (58) Torkzaban, S.; Kim, Y.; Mulvihill, M.; Wan, J.; Tokunaga, T. K. Transport and deposition of functionalized CdTe nanoparticles in saturated porous media. *J. Contam. Hydrol.* **2010**, *118*, 208–217.
- (59) Xu, S.; Gao, B.; Sayers, J. E. Straining of colloidal particles in saturated porous media. *Water Resour. Res.* **2006**, *42*, W12S16.
- (60) Taneda, S. Visualization of separating Stokes flows. *J. Phys. Soc. Jpn.* **1979**, *46*, 1935–1942.